

Integrating biomechanics into developmental plant models expressed using L-systems

Catherine Jirasek (1), Przemyslaw Prusinkiewicz (1) and Bruno Moulia (2)

(1) Department of Computer Science
University of Calgary
Calgary, Alberta, Canada T2N 1N4
e-mail: pwp@cpsc.ucalgary.ca

(2) INRA, Station d'écophysiologie des plantes fourragères
Lusignan, France

Abstract

We present a method for incorporating the biomechanical model of the bending of branch axes introduced by Schaffer and Fournier et al. into developmental plant models expressed using L-systems. The models capture the impact of gravity, tropisms, contact between elements of a plant structure and contact with obstacles on the shape of branches. Sample plants modeled using this technique are compared with photographs of real plants.

Keywords: L-system, biomechanics, elasticity, rod, gravity, tropism.

Reference

Integrating biomechanics into developmental plant models expressed using L-systems. In: H.-Ch. Spatz and T. Speck (Eds.): *Plant biomechanics 2000*. Proceedings of the 3rd Plant Biomechanics Conference, Freiburg–Badenweiler, August 27 to September 2, 2000. Georg Thieme Verlag, Stuttgart, 2000, pp. 615–624.

Integrating biomechanics into developmental plant models expressed using L-systems

C. Jirasek ¹, P. Prusinkiewicz ¹ and B. Moulia ²

¹ Department of Computer Science, University of Calgary, Alberta, Canada

² INRA, Station d'écophysiologie des plantes fourragères, Lusignan, France

Abstract

We present a method for incorporating the biomechanical model of the bending of branch axes introduced by Schaffer and Fournier *et al.* into developmental plant models expressed using L-systems. The models capture the impact of gravity, tropisms, contact between elements of a plant structure and contact with obstacles on the shape of branches. Sample plants modeled using this technique are compared with photographs of real plants.

Introduction

Plant architecture and its coupling with the environment play an essential role in the colonization of space by plants (see review in [9]). Consequently, comprehensive functional-structural plant models take into account physical, biological, and environmental processes that influence plant development. L-systems [14,15] provide a convenient theoretical and programming framework for the architectural modeling of plants, and have been used to model a variety of interactions between plants and their environment. Examples include the effects of local light on the development of the aerial architecture of plants, and the effects of water availability on root growth [9]. Nevertheless, the effects of gravity, tropisms, and contacts between organs have been captured by L-system models only in a simple manner [15]. The objective of our current work is to improve the representation of branch shape in L-system models by including the combined effects of gravity and tropisms according to the current state of the biomechanical analysis of these phenomena. Our approach is based on the model of axis growth and reorientation introduced by Schaffer [16] and Fournier *et al.* [4]. This model predicts a sigmoidal shape of branch axes by combining the notion of the gravitropic set angle (GSA) [2] with the laws of the theory of elasticity [8] applied to longitudinally and radially growing axes. In particular, it incorporates incremental changes in the amount of load-bearing material due to secondary growth, and captures the resulting “memorization” of branch shape [4,16].

A parallel technique for including biomechanical factors into architectural tree models has been proposed in the scope of the AMAP modeling system [3,5]. The biomechanical component of that model was implemented as an external module using the finite element method. In contrast, we incorporate the effects of weight and gravitropism on branch shape directly into the framework of L-systems. As a result, the system of equations that describes the biomechanical aspects of a plant becomes an inherent part of the model, and is automatically updated as the plant develops. Metaphorically speaking, the system of equations grows with the modeled plant. The proposed method makes it possible to address questions concerning plant axis shape that combine biomechanics with biological regulatory mechanisms [4,5] and with the trade-offs between various functions of the axes [12].

Mechanical model of a branch axis

We conceptualize the branch axis as an inextensible elastic rod of length L , with natural parameter $s \in [0, L]$ denoting the arc-length distance of a point \mathbf{P} from the base of the rod.

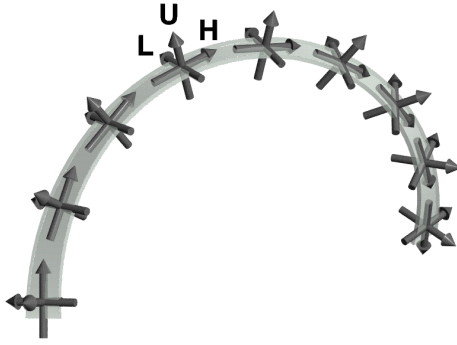


Figure 1. Local **HLU** frames of a sample rod

Each point \mathbf{P} is associated with a local frame of reference defined by mutually orthogonal unit vectors \mathbf{H} , \mathbf{L} and \mathbf{U} (heading, left, and up). We assume that vector \mathbf{H} is tangent to the rod axis and vectors \mathbf{L} and \mathbf{U} are aligned with the principal axes of the cross-section of the rod (Figure 1). In a straight prismatic rod each local reference frame will be parallel to all others. In general, two successive reference frames separated by an infinitesimal rod segment

of length ds may be rotated through an infinitesimal angular vector $d\Phi$, which characterizes the curvature and twist at point \mathbf{P} . A rod, and specifically a growing plant axis, may possess curvature and twist in the unloaded state [4]; we denote the corresponding angle of rotation at \mathbf{P} by $d\Phi$. We call $\mathbf{\Omega} = d\Phi/ds$ and $\underline{\mathbf{\Omega}} = d\Phi/ds$ the rates of rotation of the reference frame **HLU** along the rod, although s is a spatial coordinate and not time.

Given vectors $\mathbf{H}(0)$, $\mathbf{L}(0)$ and $\mathbf{U}(0)$ specifying the initial reference frame at $s=0$, the rate of rotation $\mathbf{\Omega}$ determines the reference frame **HLU** at any point on the rod as the solution to the differential equations:

$$d\mathbf{H}/ds = \mathbf{\Omega} \times \mathbf{H}, \quad d\mathbf{L}/ds = \mathbf{\Omega} \times \mathbf{L}, \quad d\mathbf{U}/ds = \mathbf{\Omega} \times \mathbf{U}. \quad (1-3)$$

Since all vectors $\mathbf{H}(s)$ have unit length and are tangent to the axis at points $\mathbf{P}(s)$, $s \in [0, L]$, the axis shape is given by the integral:

$$\mathbf{P}(s) = \mathbf{P}(0) + \int_0^s \mathbf{H}(s) ds. \quad (4)$$

To calculate the rates of rotation $\mathbf{\Omega}$ that determine the shape of the rod at a static equilibrium, we compare the internal moments ${}^I\mathbf{M}$, resulting from the reaction of the material to deformation, and external moments \mathbf{M} acting on all points \mathbf{P} of the rod. Let us consider the internal moments first. The infinitesimal rotations are vectors, thus the rotation rates are vectors as well, and can be decomposed along the axes $\mathbf{H}\mathbf{L}\mathbf{U}$:

$$\mathbf{\Omega}_H = \mathbf{\Omega} \cdot \mathbf{H}, \quad \mathbf{\Omega}_L = \mathbf{\Omega} \cdot \mathbf{L}, \quad \mathbf{\Omega}_U = \mathbf{\Omega} \cdot \mathbf{U}, \quad (5)$$

$$\underline{\mathbf{\Omega}}_H = \underline{\mathbf{\Omega}} \cdot \mathbf{H}, \quad \underline{\mathbf{\Omega}}_L = \underline{\mathbf{\Omega}} \cdot \mathbf{L}, \quad \underline{\mathbf{\Omega}}_U = \underline{\mathbf{\Omega}} \cdot \mathbf{U}. \quad (6)$$

Since \mathbf{L} and \mathbf{U} are the principal axes of the cross-section of the rod, its elastic properties at \mathbf{P} are captured by the torsional rigidity C_H and the flexural rigidities in the planes $\mathbf{H}\mathbf{U}$ and $\mathbf{H}\mathbf{L}$, denoted C_L and C_U , respectively. The moment ${}^I\mathbf{M}$ due to the local deformation of the rod at \mathbf{P} is equal to

$${}^I\mathbf{M} = {}^I M_H \mathbf{H} + {}^I M_L \mathbf{L} + {}^I M_U \mathbf{U}, \quad (7)$$

where:

$${}^I M_H = C_H (\underline{\mathbf{\Omega}}_H - \mathbf{\Omega}_H), \quad {}^I M_L = C_L (\underline{\mathbf{\Omega}}_L - \mathbf{\Omega}_L), \quad {}^I M_U = C_U (\underline{\mathbf{\Omega}}_U - \mathbf{\Omega}_U). \quad (8-10)$$

By substituting equations (5-6) into (8-10) and then into (7), we obtain:

$${}^I\mathbf{M} = C_H ((\underline{\mathbf{\Omega}} - \mathbf{\Omega}) \cdot \mathbf{H}) \mathbf{H} + C_L ((\underline{\mathbf{\Omega}} - \mathbf{\Omega}) \cdot \mathbf{L}) \mathbf{L} + C_U ((\underline{\mathbf{\Omega}} - \mathbf{\Omega}) \cdot \mathbf{U}) \mathbf{U}, \quad (11)$$

or, in dyadic notation,

$${}^I\mathbf{M} = (\underline{\mathbf{\Omega}} - \mathbf{\Omega}) \cdot \mathbf{S}, \quad \text{where } \mathbf{S} = C_H \mathbf{H}\mathbf{H} + C_L \mathbf{L}\mathbf{L} + C_U \mathbf{U}\mathbf{U}. \quad (12-13)$$

Let us denote by \mathbf{K} the external force per unit length, acting on the rod at \mathbf{P} . The accumulated force \mathbf{F} and the moment \mathbf{M} caused by the “overhanging” rod segment $[s, L]$ acting on the rod at \mathbf{P} satisfy the equations [8]:

$$d\mathbf{F}/ds = -\mathbf{K} \quad \text{and} \quad d\mathbf{M}/ds = \mathbf{F} \times \mathbf{H}. \quad (14-15)$$

At a static equilibrium, the equation

$$\mathbf{M} + {}^I\mathbf{M} = \mathbf{0} \quad (16)$$

must be satisfied at each point \mathbf{P} of the rod.

Differential equations (1-3,14-15), complemented with the algebraic equations (12,16), represent a two-point boundary problem with the unknown vectors \mathbf{H} , \mathbf{L} , \mathbf{U} , $\mathbf{\Omega}$, ${}^I\mathbf{M}$, \mathbf{F} , and \mathbf{M} . We solve these equations numerically using a simple relaxation technique. To this end, we divide the rod into short segments of length Δs_i , where index i ranges from 0 at the proximal (fixed) end of the rod to n at the distal (free) end, and apply the following algorithm:

Input: Vectors $\mathbf{H}(0)$, $\mathbf{L}(0)$, and $\mathbf{U}(0)$ that define the orientation of the $\mathbf{H}\mathbf{L}\mathbf{U}$ frame at the proximal end of the rod, force $\mathbf{F}(L) = \mathbf{0}$ and moment $\mathbf{M}(L) = \mathbf{0}$ at the free end, external force densities \mathbf{K}_i , rotation rates $\underline{\mathbf{\Omega}}_i$ that define the shape of the rod in the unloaded state, and the initial values of the rotation rates $\mathbf{\Omega}_i$ (for example, all equal to $\underline{\mathbf{\Omega}}_i$).

Output: The shape of the rod at a static equilibrium.

Step 1. Compute the orientation of the frame $\mathbf{H}\mathbf{L}\mathbf{U}$ at each point of the rod using a discretized version of equations (1-3). Since the orientation of the

frame at the proximal end of the rod is known, computation proceeds *outwards* from the proximal to the distal end, according to the formula:

$$\mathbf{H}_{i+1}^t = \mathbf{H}_i^t + \mathbf{\Omega}_i^t \times \mathbf{H}_i^t \Delta s_i, \quad i = 0, \dots, n-1, \quad (17)$$

and analogous formulae for \mathbf{L}_{i+1}^t and \mathbf{U}_{i+1}^t .

Step 2. Compute the distribution of the external forces and moments along the rod using a discretized version of equations (14-15). Since the boundary values at the distal end of the rod are known, computation proceeds *inwards* from the distal to the proximal end according to the formulae:

$$\mathbf{F}_{i-1}^t = \mathbf{F}_i^t + \mathbf{K}_i \Delta s_i, \quad i = n, \dots, 1, \quad (18)$$

$$\mathbf{M}_{i-1}^t = \mathbf{M}_i^t + \mathbf{H}_i^t \times \mathbf{F}_i^t \Delta s_i. \quad i = n, \dots, 1. \quad (19)$$

Step 3. Compute the unbalanced moments at nodes i between segments Δs_i and Δs_{i+1} using a combination of formulae (12,13,16):

$$\mathbf{E}_i^t = \mathbf{M}_i^t + {}^t\mathbf{M}_i^t = \mathbf{M}_i^t + (\mathbf{\Omega}_i - \mathbf{\Omega}_i^t) \cdot (C_H \mathbf{H}\mathbf{H} + C_L \mathbf{L}\mathbf{L} + C_U \mathbf{U}\mathbf{U}), \quad (20)$$

then adjust the rotation rates $\mathbf{\Omega}_i$ proportionally to these unbalanced moments:

$$\mathbf{\Omega}_i^{t+1} = \mathbf{\Omega}_i^t + k \mathbf{E}_i^t, \quad i = 0, \dots, n-1. \quad (21)$$

The parameter k is an empirically chosen constant that controls the speed of convergence to the solution.

Step 4. Repeat steps 1-4 until the magnitude of all unbalanced moments $|\mathbf{E}_i|$ decreases below a threshold value, then compute the shape of the rod using a discretized counterpart of equation (4):

$$\mathbf{P}_{i+1} = \mathbf{P}_i + \mathbf{H}_i \Delta s_i. \quad \square \quad (22)$$

The two-way information flow inherent in this algorithm has been described in the context of the analysis of chainlike robotic manipulators by Craig [1]. It is the cornerstone of the integration of mechanical phenomena into developmental models of plant architecture.

Model expression using L-systems

We assume that the reader is familiar with the formalism of L-systems and its application to the modeling of plant architecture, as described, for example, in [14,15]. The concept of computing numerical solutions of differential equations using L-systems is further discussed in [6].

An L-system captures the development of a plant using *rewriting rules* or *productions*. For example, the rule $\mathbf{A} \rightarrow \mathbf{IA}$ may be used to specify that at given time intervals an apex \mathbf{A} will produce an internode \mathbf{I} and recreate itself at the distal end of this internode. A repetitive application of this rule yields an axis composed of a sequence of internodes:

$$\mathbf{A} \Rightarrow \mathbf{IA} \Rightarrow \mathbf{IIA} \Rightarrow \mathbf{IIIA} \Rightarrow \mathbf{IIIIA} \Rightarrow \dots \quad (23)$$

Plant modules, such as the apex and the internodes, can be characterized using numerical parameters. Let us consider a simple example of a develop-

ing axis in which all internodes have the same length Δs and are subject to the same force \mathbf{K} per unit length. We assume that the vectors \mathbf{H} , \mathbf{U} and \mathbf{K} are coplanar, thus the axis will bend in the plane \mathbf{HU} perpendicular to \mathbf{L} . We also assume that the rigidity C_L is constant. An internode \mathbf{I} is then completely specified by vector \mathbf{H} , rotation rate $\mathbf{\Omega}$, external force \mathbf{F} and external bending moment \mathbf{M} . If all these parameters are assigned the initial value of $\mathbf{0}$, the production $\mathbf{A} \rightarrow \mathbf{IA}$ will become $\mathbf{A} \rightarrow \mathbf{I}(\mathbf{0}, \mathbf{0}, \mathbf{0}, \mathbf{0})\mathbf{A}$. The algorithm for computing the shape of the rod in equilibrium can be then expressed as follows:

Step 1. The outward propagation of orientations in a sequence of internodes (equation 17) is implemented by production

$$\mathbf{I}(\mathbf{H}_l, \mathbf{\Omega}_l, \mathbf{F}_l, \mathbf{M}_l) < \mathbf{I}(\mathbf{H}, \mathbf{\Omega}, \mathbf{F}, \mathbf{M}) \rightarrow \mathbf{I}(\mathbf{H}_l + \mathbf{\Omega}_l \times \mathbf{H}_l \Delta s, \mathbf{\Omega}, \mathbf{F}, \mathbf{M}),$$

where symbol $<$ separates the left context from the strict predecessor of the production [14,15]. This production states that the header vector \mathbf{H} in the module $\mathbf{I}(\mathbf{H}, \mathbf{\Omega}, \mathbf{F}, \mathbf{M})$ will acquire a new direction, calculated as a function of the header vector \mathbf{H}_l and the rotation rate $\mathbf{\Omega}_l$ in the previous internode.

Step 2. The inward propagation of external forces and moments (equations 18 and 19) is expressed by production

$$\mathbf{I}(\mathbf{H}, \mathbf{\Omega}, \mathbf{F}, \mathbf{M}) > \mathbf{I}(\mathbf{H}_r, \mathbf{\Omega}_r, \mathbf{F}_r, \mathbf{M}_r) \rightarrow \mathbf{I}(\mathbf{H}, \mathbf{\Omega}, \mathbf{F}_r + \mathbf{K}_r \Delta s, \mathbf{M}_r + \mathbf{H}_r \times \mathbf{F}_r \Delta s),$$

where symbol $>$ separates the strict predecessor from the right context.

Step 3. The remaining computations (equations 20 and 21) are performed under the simplifying assumption of the planar deformation of the rod. The unbalanced moment is then reduced to $\mathbf{M} + C_L \mathbf{\Omega}$, and the updated rotation rate $\mathbf{\Omega}$ is captured by production:

$$\mathbf{I}(\mathbf{H}, \mathbf{\Omega}, \mathbf{F}, \mathbf{M}) \rightarrow \mathbf{I}(\mathbf{H}, \mathbf{\Omega} + k(\mathbf{M} + C_L \mathbf{\Omega}), \mathbf{F}, \mathbf{M}).$$

In the complete L-system, these productions are guarded by conditions that ensure proper sequencing of the production applications (*Step 4*) and schedule the addition of new segments by the apex. Details are given in [7].

In general, the assignment of parameters to the internodes provides a mechanism for automatically increasing the number of variables that describe the plant as it grows. Variables in the neighboring modules are accessed using context-sensitive productions. Since L-systems can capture the development of branching structures and the information flow between their modules, the described technique extends from individual axes to entire plants.

Secondary growth, tropisms, and collisions

Radial (secondary) growth is simulated according to the pipe model [17], which postulates that the vascular strands originating in a newly added segment contribute to the girth of previous segments. In other words, the addition of a distal internode of cross-section A causes the addition of external layers of the same area to all preceding segments. Together the primary and secondary growth modify [4,16]:

- The linear density of the external forces \mathbf{K} . For example, if the external forces are due exclusively to the axis weight, then $\mathbf{K} = A\rho\mathbf{g}$, where A is the area of the cross-section of the stem at a given point P , ρ is the average density of the stem material at this cross-section, and \mathbf{g} is the acceleration of gravity.
- The torsional and flexural rigidities $C_H = GJ$, $C_L = EI_L$ and $C_U = EI_U$, where G is the shear modulus of the stem material, E is its Young's modulus, J is the torsional constant, and I_L and I_U are the second moments of area of the stem's cross-section. The values of constants J , I_L and I_U for different cross-sectional geometries are listed in [12].
- The curvature and twist of the branch axis at rest $\underline{\Omega}$. Assuming that the principal axes of the cross-section of a new annual layer are aligned with the principal axes of the previous cross-section, each component of the rate of rotation at rest $\underline{\Omega}'$ is calculated as a weighted average of the previous rotation at rest $\underline{\Omega}$ and the current rotation vector $\underline{\Omega}$, e.g.:

$$\underline{\Omega}'_L = (C_L\underline{\Omega}_L + C'_L\underline{\Omega}_L) / (C_L + C'_L). \quad (24)$$

The constants C_L and C'_L denote the rigidities of the previous branch axis and of the newly added layer, respectively.

Equation (24) is based on the observation that a new layer added by secondary growth is “molded” on the existing branch segment, and thus may have different rest curvature and twist than previous layers [4,16]. The new rate of rotation $\underline{\Omega}'$ (curvature and twist) of an axis segment at rest represents the auto-stress equilibrium between the new layer and the existing core within the segment's cross-section. Thus, the rest shape of an axis after a step of secondary growth partially memorizes the actual shape of this axis under load. A derivation of equation (24) is included in [7]. It is an alternative but equivalent formulation to that proposed in [4].

The secondary growth is incorporated into the model as follows. After a step of longitudinal growth, the girth of all internodes is recalculated according to the pipe model. The propagation of information from the distal to the proximal end, postulated by the pipe model, is implemented by right-context-sensitive productions. The rotation rates at rest and the rigidities of each internode are computed using the formulae described above and incorporated into an L-system production. The new mechanical equilibrium is then determined as discussed in the preceding sections for an axis without secondary growth. This cycle is repeated for each new internode produced by the apex.

Further extensions of the model include tropisms and collisions. Tropisms are simulated by rotating the frame of the newly inserted segment so that its tangent vector \mathbf{H} becomes more closely aligned with the direction of a predefined tropism vector \mathbf{T} . Contacts between structural elements (for example, grapes in a bunch) and between the structure and its environment (e.g., branches partially laying on the ground) are simulated under the assumption that the colliding elements are elastic, and act on each other with forces proportional to the depth of penetration (penalty method [13].) This technique makes it possible to approximate the effect of contact on the deformation of the axes, although it is not precise enough to predict the local shape of the contact zone in the organs resting on each other.

Results

The described biomechanical model was applied to simulate the development and capture the structure of several plants. The simulations were carried out using the plant simulation software *cpfg* with open L-system support [9]. The open L-system extension was used to exchange forces between parts in contact. A complete implementation of the L-system models is presented in [7].

Figure 2 compares the S-shaped branches of a tree with the results of a simulation. The branches in the model bend downward due to their weight, but the branch tips arch upward due to a vertically oriented tropism vector. Figure 3 shows the results of simulating a hanging plant using the same model with different parameters. In the model of *Spiraea* sp. (Figure 4), twigs arch downward due to gravity, whereas the flower-bearing shoots stand upright due to a strong orthogravitropism. Figure 5 illustrates the effect of contact between fruits on the shape of fruit stems. The stems were assumed to elongate and increase in diameter uniformly throughout their length, with no new segments added during the simulation. Two applications of this model are shown in Figure 6. Figure 7 illustrates schematically the effect of contact with the ground on the shape of a growing axis affected by tropism. The same model without tropism was formally applied to recreate a cycad (Figure 8), with the leaves prevented from penetrating the ground plane by the collision-detecting mechanism.



Figure 2: A photograph and a model of S-shaped tree branches. The branches bend down due to gravity, but arch upward at the distal ends due to a tropism.

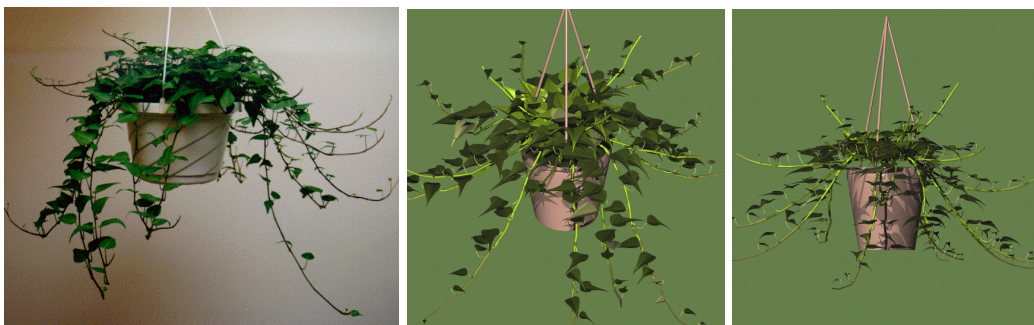


Figure 3: A photograph and two views of a model of a hanging plant. Branches hang down due to gravity, but are also influenced by an upward tropism.



Figure 4: A photograph, a model and a zoom into the modeled flower-bearing shoots of a *Spiraea* shrub. The twigs arch downward due to gravity, the flower-bearing shoots stand upright due to simulated orthogravitropism.

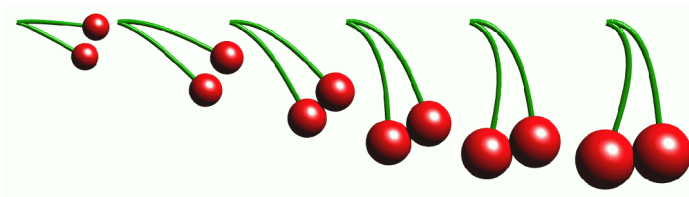


Figure 5: Growing cherries. The stems bend down as the fruits become heavier.

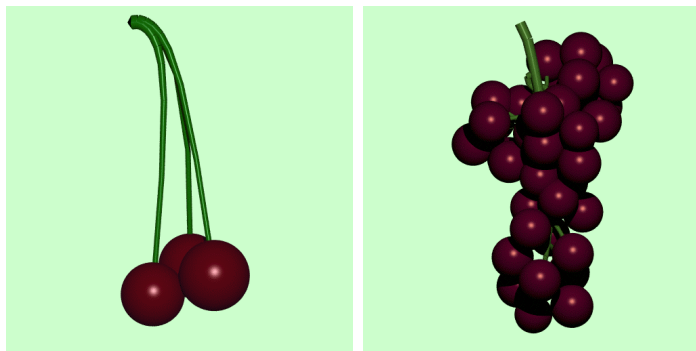


Figure 6: Models of cherries and grapes. The individual fruits rest against each other.

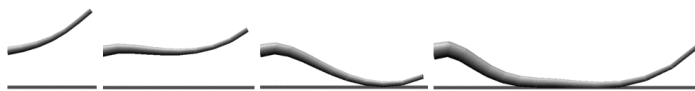


Figure 7: A growing orthotropic axis collides with the ground.



Figure 8: A photograph and two views of a model of a cycad. The lower leaves lie on the ground plane.

In plants and organs without organized secondary growth (*e.g.*, Figures 5 and 8), biomechanical effects of growth are manifested by diffuse primary radial expansion and secondary cell wall deposition, rather than the addition of external rings of cells. Nevertheless, processes of shape memorization have been reported in herbs [10] and the biomechanical principle involved is probably similar [11]. Therefore, we have applied equation (24) to qualitatively capture the shape memorization mechanism even in the absence of detailed information concerning the distribution of growth rates within the cross sections.

Conclusions

The described model makes it possible to visually capture the shape of branches resulting from the combined effect of weight, tropisms, and contact of organs with each other and with obstacles in the environment. The incorporation of biomechanics into L-systems makes it possible to explore different branching architectures relatively easily. Prospective extensions and applications of the model include: (a) incorporation of a mechanistic model of tropisms that associates bending of branch axes to differential growth; (b) simulation of the biological regulation of reaction wood formation, and its mechanical effects; and (c) testing of biological hypotheses relating plant architecture to biomechanics, for instance the impact of stresses in the mother branch axis on the formation of lateral branches.

Acknowledgments

The support for this work by a research grant, a postgraduate scholarship, and an equipment grant from the Natural Sciences and Engineering Research Council of Canada is gratefully acknowledged.

References

- [1] J. J. Craig (1989): *Introduction to robotics: mechanics and control*. Second edition. Addison-Wesley, Reading, 1989.
- [2] J. Digby and R. D. Firm (1995): The gravitropic set-point angle (GSA): the identification of an important developmentally controlled variable governing plant architecture. *Plant, Cell and Environment*, 18: 1434-1440.
- [3] Th. Fourcaud (1997): Relations entre croissance et biomécanique de l'arbre. In: J. Bouchon, Ph. de Reffye and D. Barthélémy (Eds.): *Modélisation et simulation de l'architecture des végétaux*. INRA Editions, Paris, pp. 350-382.
- [4] M. Fournier, H. Bailleres, and B. Chanson (1994): Tree biomechanics: growth, cumulative prestresses, and reorientations. *Biomimetics*, 2 (3): 229-251.

- [5] J. Gril, F. Blaise and M. Fournier (1992) Introduction de concepts mécaniques dans un logiciel de croissance des plantes. In: B. Thibaut (Ed.): *Architecture, Structure, Mécanique de l'Arbre IV*. LMGC, Montpellier, pp. 171-185.
- [6] M. Hammel and P. Prusinkiewicz (1996): Visualization of developmental processes by extrusion in space-time. *Proceedings of Graphics Interface '96*, pp. 246-258.
- [7] C. Jirasek (2000): A biomechanical model of branch shape in plants expressed using L-systems. M.Sc. Thesis, Department of Computer Science, University of Calgary.
- [8] L. Landau and E. Lifshitz (1986): *Theory of elasticity*. Third edition. Butterworth Heinemann, Oxford.
- [9] R. Mech and P. Prusinkiewicz (1996): Visual models of plants interacting with their environment. *Proceedings of SIGGRAPH '96*, pp. 397-410.
- [10] B. Moulia., M. Fournier and D. Guitard (1994): Mechanics and form of the maize leaf : in vivo qualification of the flexural behaviour. *J. Mater. Sci.*, 29 : 2359-2366.
- [11] B. Moulia (1993) *Etude mécanique du port foliaire du maïs (Zea mays L.)*. Thèse de l'Université de Bordeaux I (UFR de Physique). 123pp.
- [12] K. Niklas (1992): *Plant biomechanics*. The University of Chicago Press, Chicago.
- [13] J. Platt and A. Barr (1988): Constraint methods for flexible models. *Computer Graphics*, 22 (4): 279-288.
- [14] P. Prusinkiewicz, M. Hammel, J. Hanan and R. Mech (1997): Visual models of plant development. In: G. Rozenberg and A. Salomaa (Eds.): *Handbook of formal languages*, Vol. III, Springer, Berlin, pp. 535-597.
- [15] P. Prusinkiewicz and A. Lindenmayer (1990): *The algorithmic beauty of plants*. Springer, New York.
- [16] B. Schaffer (1990) Forme d'équilibre d'une branche d'arbre. *CR Acad. Sci. Paris*, 311 (2): 37-43.
- [17] K. Shinozaki, K. Yoda, K. Hozumi and T. Kira (1964): A quantitative analysis of plant form - the pipe model theory. I. Basic analyses. *Japanese Journal of Ecology*, 14 (3): 97-104.